Impact of Columnar Grains & Porosity on Fatigue Performance of Aluminum Castings

Robert Mackay, Anthony Lombardi & Glenn Byczynski
Nemak US, Southfield, Michigan, USA

ABSTRACT

Laboratory life-to-failure methods, used to estimate aluminum casting fatigue durability, is critical for establishing intended lifespan service conditions. The Over-Stress Probe (OSP) method, which is widely used in academia and industry, has benefits and drawbacks in adequately providing a lifespan estimation. Normally, when an OSP protocol is followed, not all fatigue test samples are examined with fractography. Only a fatigue performance value is cited with any failures driving additional fatigue sample testing which contributes to delays and cost overruns for casting launch programs. Instead, the authors have utilized a more complete fractographic examination to help process developers understand the role of the casting parameters on fatigue performance. The authors have taken this approach in this manuscript on an OSP test regime which includes a total of 66 fatigue samples, all with fractographic observations of the flaw characterization and size that nucleated the fatigue fracture.

Keywords: fatigue, aluminum castings, columnar grains, porosity

INTRODUCTION

Axial fatigue testing at elevated temperatures is the most common approach to estimate lifespan conditions for castings made using Gravity Semi-Permanent Mold (GSPM), High Pressure Die Casting Process (HPDC) and the Precision Sand Casting Process (PSCP).[1] The elevated temperature regime used for axial fatigue testing (typically 120−150C/248−302F) is meant to closely replicate its service conditions. As many castings experience cyclical tension and compressive loading conditions, an axial fully reversed ($R = \sigma_{max}/\sigma_{min} = -1$) fatigue test is used.

Axial fatigue failure, from nucleation until complete fracture, is covered by three regimes. High Cycle Fatigue (HCF) is usually defined as a test sample that has initially experienced cyclic plastic deformation at low alternating stress levels ($\leq 10^5$).[1-6] The life of a fatigue crack (N_{tctf} = total cycles to failure) may be defined as follows in Equation 1.[7]

$$N_{tctf} = N_i + N_p + N_f \qquad \textbf{Eqn. 1}$$

Where:
N_i = the number of cycles required to initiate a crack (associated with stress concentrator).

N_p = the number of cycles required to propagate the crack (slow fracture region).

N_f = the number of cycles to failure, which is usually insignificant since it occurs so rapidly (fast fracture).

Figure 1 shows a schematic of the fatigue fracture surface and a representative scanning electron microscopy/back scattered electron (SEM/BSE) image that illustrates the three main stages of the complete fatigue fracture. The longest portion of the total fatigue test sample life is tied up in a parameter that reflects the number of cycles to nucleate a fatigue crack (N_i). Typically, the sites that initiate a fatigue crack, be it a pore, an oxide, etc., are usually near the surface of a fatigue test sample's reduced gauge section due to its stress amplification effect. Historically, most of the failures (or the start point for N_i) are due to micro-shrinkage pores which have nucleated from a bi-film during the solidification process.[3,6-8] While the size of these micro-shrinkage pores plays a role on over all fatigue life, the position of the pore itself with respect to the polished reduced gauge section is also a factor.

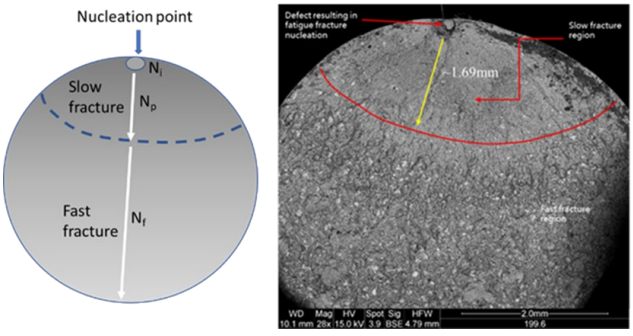

Figure 1. Example of a fracture surface of an axial fatigue fracture surface representing the fatigue fracture nucleation, slow fracture stage and the fast fracture stage. The SEM/BSE image is from a completed and examined axial fatigue test from Mackay et. al.[7]

Boileau[5,6] indicated that a similarly sized micro-shrinkage pore at the surface versus the interior of the reduced gauge cross-section of the fatigue sample will not have similar lives. This is due to the stress concentration effect of a sharp edge (the outer most extension of a micro-shrinkage pore perpendicular to the axial loading direction) being more significant if located near the surface of the reduced gauge section. In contrast, a micro-shrinkage pore in the interior of the sample has this stress concentration deflected at two edges, resulting in a lower local stress amplification effect. Thus, the time required to start fatigue crack propagation from an interior micro-shrinkage pore takes longer.

EXPERIMENTAL METHDOLOGY

ELEVATED TEMPERATURE AXIAL FATIGUE TEST

The total number of fatigue samples for the OSP protocol was 66 (Each fatigue bar was extracted from one of 66 individual castings that use the Nemak-Cosworth™ Precision Sand Casting Process/PSCP.[7-11] Figure 2 shows the dimensions used to fabricate the 66 fatigue test bars.

Fatigue test sample testing was carried out as per the ASTM E 466-96 protocol. TestStar™ IIs fatigue software by MTS was used to monitor the sinusoidal axial fatigue at a frequency of 98Hz. The stress ratio was R = -1, ($R = \sigma_{min}/\sigma_{max}$). Maintaining a test temperature of 150C (302F) was done using a resistance heater tape material (Omega) which was in direct contact with the test specimen. Temperature was monitored by a K-type thermocouple that was held in place on the reduced gauge section using 3M glass fiber electrical tape. Typically, it took between 3 and 5 minutes for the reduced gauge section to reach the target temperature.

The alignment process of the fatigue test frame was performed to address two types of possible misalignment—concentric and angular. The fatigue test frames are equipped with an alignment collar (MTS Model 609) that allows alignment in conjunction with a specimen fitted with 12 strain gauges that is connected to a computerized alignment data acquisition and analysis system (MTS 709). This is the system that is used to align the fatigue frames in accordance with ASTM E1012-05.

Once a test sample failure has occurred, and prior to the start of another fatigue test, the nucleation point of the fracture surface with respect to the load frame orientation (clock position), along with the distance from the center of the reduced gauge section where the fracture occurred, and the resulting diameter of the reduced gauge section at the fracture point, was documented. Inconsistency in these orientation values will necessitate a check of the frame alignment as mentioned earlier.

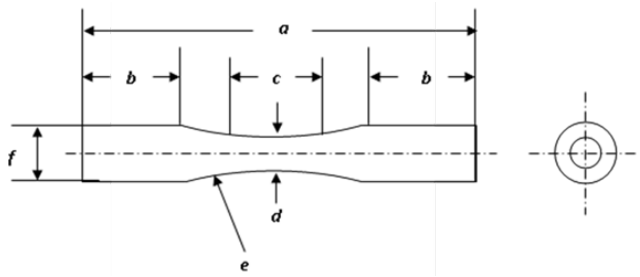

Fatigue Sample Feature	a	b	c	d	e	f
(mm)	127.0	28.5	16.0	8.0	63.75	15.0

Figure 2. Dimensions of the Fatigue test sample fabrication as outlined in ASTM E 466-96.

OVER STRESS PROBE PROTOCOL

Each fatigue test was used to plot the fatigue total life until failure, also known as the Over Stress Probe (OSP) method, which can be described as follows:

The initial life goal of 10^7 cycles was set and the initial alternating stress was 82 MPa (note some specifications may use lower or higher initial alternating stress). Should the fatigue test sample survive the initial 10^7 cycles without failure, the test is considered a pass and the same fatigue test sample in the same test frame will then have the alternating stress increased by 10% (increment of 8.2 MPa, or 90.2 MPa) and then run an additional 10^6 cycles. Should the fatigue test sample survive that stage then the alternating stress is increased a further increment of 8.2 MPa, or 98.4 MPa, for another 10^6 cycles. This incremental testing strategy is continued until actual fatigue failure occurs.

Results of a completed OSP regime may be represented as a percentage of the total life. A sample surviving the initial stage is considered 100% (Stress Time Percent statistic/STP). Since the subsequent (secondary) testing is at 10^6 cycles, the survival is an extra 10%, or 110% at 82 MPa. Should the sample fail the secondary stage at 500,000 cycles, then the final test result would be 105% at 82 MPa. The authors will represent a completed OSP as the total number of cycles completed when fracture occurred as this may be easier to represent the large amount of data used in this manuscript.

The purpose for using a step increment in stress and a smaller number of alternating cycles (10^6) after achieving the compliance threshold (10^7 cycles at 82 MPa), instead of just running at 82 MPa until failure, is time and cost. Using an 8.2 MPa increment in alternating stress for each surviving 10^6 regime is meant to shorten the test time and allow one axial fatigue test frame to conduct more tests.

CHEMISTRY, METALLOGRAPHY & FRACTOGRAPHY METHODOLOGY

Fractography of fatigue test sample fracture surfaces was performed using a Keyence VHX-6000 stereomicroscopy system. A calibration scale micrometer (S/N: SM-2-0064, 99.8µm measured against a 100µm scale) was used to check magnification settings so that nucleating flaw dimensions (min. and max. length) were determined accurately.

Fatigue samples were polished to perform metallography analysis in a vertical plane just below the fracture surface (Fig. 3). It should be noted that a 2-D cross-section of a metallographic examination may under-represent the size of the critical pore/artifact that nucleates fatigue but can show if the process in terms of melt quality, chemistry and solidification was consistent within the samples in the current fatigue OSP protocol. This will become a critical aspect towards the arguments made at the end of the manuscript.

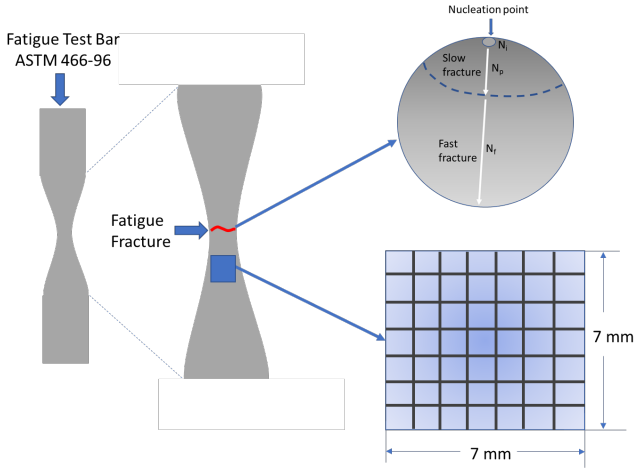

Figure 3. Schematic of the fatigue test bar, fracture location and the determinate fractography (stereomicroscopy) and light optical microscopy (porosity and λ_2 analysis).

Metallography was conducted on an Olympus IX70 Light Optical Microscope system. Porosity and Secondary Dendrite Arm Spacing (λ_2) was done with the aid of an Image Analysis software by CLEMEX (Version 3.5.020 F). Percent Porosity (%) assessment was performed on a 49-field grid array (7 mm x 7 mm) at a magnification of 50x. While standard deviation for porosity measurements can be included, they will not be in this manuscript as they potentially add confusion to the graphing (e.g., σ can be several times larger than mean and a negative σ can extend below a zero value which is meaningless). The length measurement to support λ_2 determination was checked against the same calibration scale micrometer (S/N: SM-2-0064, 99.6µm measured against a 100µm scale). At a magnification of 50x several lines were drawn which orthogonally intersect at least 5 to 6 secondary dendrites.

Finally, to understand the grain structure of the casting section from which the fatigue test samples are extracted, bulkheads were polished and etched (Kellers reagent: 2ml HF, 3ml HCI, 5ml HNO_3 and 175 ml H_2O) to measure the size of the columnar grains which extend from the contact chill that's used in the Cosworth-Nemak™ process. The chemistry range of the alloy used is shown in Table 1. The alloy composition was measured using a calibrated Optical Emission Spectrometer (OES) and verified using SAX 329-B, supplied by Arconic, whose composition is a product registered only for Nemak.

Table 1. Upper and Lower Limits for Alloy used in this Fatigue Study

Si	Fe	Cu	Mn	Mg	Ni	Zn	Ti
9.0	0.6	3.0	0.4	0.3	0.05	0.7	0.2
8.0	-	2.6	-				

RESULTS

MICROSTRUCTURE CONSISTENCY OF THE REDUCED GAUGE SECTION OF THE FATIGUE TEST SAMPLE

Before reviewing and discussing fatigue performance in this manuscript, it's important to establish the repeatability of the microstructure found in the fatigue test samples used in the current study. A total of 20 fatigue samples from the 66 OSP data set were sectioned, as shown in Figure 3, to collect both porosity (%) and λ_2. Figure 4 shows the trend for λ_2 of the 20 selected samples and that values ranged from 20 to 24 µm which shows a good consistency in terms of overall solidification time (e.g. $\lambda_2 = 10.85 t_f^{0.30}$ [Ref. 12], where t_f is the local solidification time, which translates to 8 to 12 seconds for full solidification). Figure 4 also shows the result of the measured porosity from fatigue reduced gauge section (1 mm below the fracture surface) and shows that porosity is between 0.005 and 0.30%.

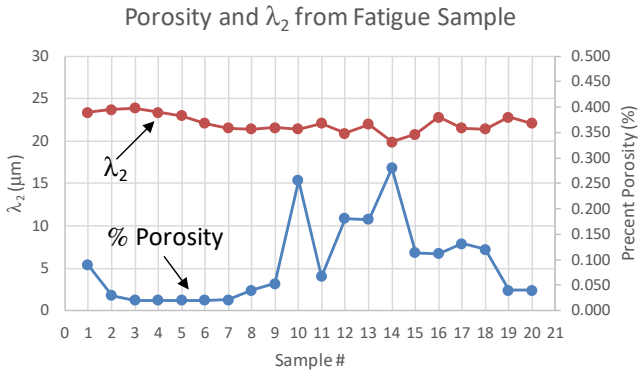

Figure 4. Summary of the λ_2 and porosity values from 20 of the 66 fatigue test bar samples.

The etched cast structure from where the fatigue bar is extracted is shown, with in-mold Tibor added in Figure 5a, and without Tibor added in Figure 5b. There is a marked difference in the size of the columnar zone which radiates from the cast iron chill. This means that depending on the position of the fatigue bar with respect the columnar field (insets in Figs. 5a and 5b) of the cast structure suggests that it is possible to have these columnar grains as part of the extracted fatigue sample.

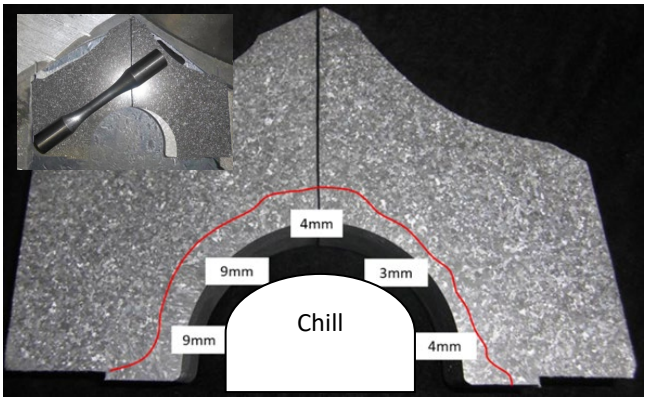

Figure 5a. The etched bulkhead with Tibor (Al-5Ti-B) added to the runner system.

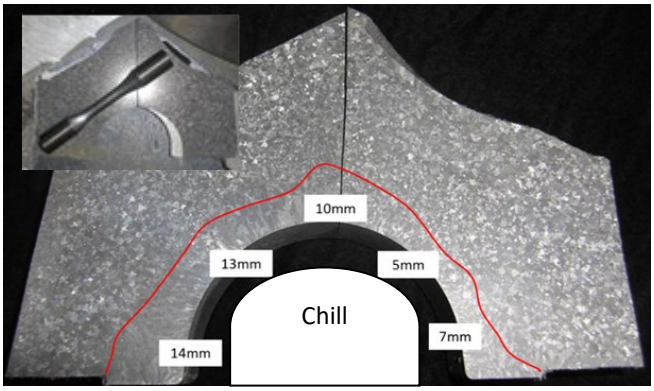

Figure 5b. The etched bulkhead without Tibor (Al-5Ti-B) added to the runner system.

Comparing Figures 5a and 5b, the columnar region on the left side of the etched casting section at its maximum extends 14 mm without in-mold Tibor. The addition of in-mold Tibor reduced the size of the columnar region to 9 mm. This is the same left side in where the fatigue test bar was extracted.

Figure 6 shows the complete results summary of the 66 sample OSP test ranging from the fatigue test bar with the shortest life (left) up to the longest life (right) all with fractographic examination. The red diamonds reflect the longest dimension of the flaw that resulted in fatigue failure. The bar graph, which reflects overall fatigue life before failure, is color coded because not all nucleation events are micro-shrinkage pores (light blue bars). There are 10 of the 66 fatigue test samples, which upon fractographic examination, did not have an observed micro-shrinkage pore as part of the nucleation event, and instead was due to a columnar grain (dark blue bars).

The observation of columnar grains may not be a highly unusual observation for fatigue crack nucleation in castings. However, as mentioned, complete fractography is normally not done on all or even most failed fatigue test samples. This is an observation that is most likely caught because all fatigue samples underwent this fractographic examination.

Also indicated on Figure 6 is the location of the micro-shrinkage pore which was not at the surface of the fatigue test sample reduced gauge section. There is a total of 5 such samples which had their fatigue nucleation site occur between 0.2 mm to 0.3 mm from the polished surface. This is worth pointing out as the authors in a previous publication[7] have shown, that comparing to the Staircase method for fatigue performance assessment, many samples run-out and as a result, never have a facture surface for examination to confirm why it survived 10^7 cycles at its alternating stress. In their work[7] they confirmed that either the pore would have to be very small, or is sufficiently located away from the polished surface, something only possible to observed from fatigue samples within the OSP trial.

Figures 7a through to 7e show examples of stereomicrographs of the fatigue fracture surfaces reflecting both porosity and columnar grains as the critical flaw that initiated the fatigue failure. Figure 7a shows the 3rd ranked fatigue sample (16% STP) which had a small pore at the polished fatigue reduced gauge section. Figure 7b shows the 4th ranking fatigue sample (24% STP) which also had a small pore as its fatigue crack nucleation event.

Figure 7c shows the 24th ranked OSP sample (123% STP) which did ultimately fail to what appears to be a columnar grain in the nucleation site. The columnar grain is characterized as a relatively flat surface with secondary

dendrite cells which appear to be non-orthogonal to the primary dendrite stem.

Figure 7d shows the 34th ranked OSP sample (129% STP) which had two micro-shrinkage pores which acted as a fatigue multi-nucleation site. This observation has been reported before and will happen as two pores maybe close to one another and at or near the surface of the polished reduced gauge section.

Figure 7e shows the fracture surface of the 49th ranked OSP sample (136% STP) which also has a columnar grain as the nucleation site. The columnar grain in fact, extends almost 2.5 mm from the surface, occupying almost approximately 30% of the whole fracture surface.

Finally, in Figure 7f, the best sample in terms of fatigue life is shown (173% STP, ranked at #66 and has only one small gas bubble at the fatigue reduced gauge section surface).

DISCUSSION

In this manuscript the authors set out to show that conducting fractography analysis on all fatigue test samples from a multi-sample fatigue test protocol will provide a more complete understanding of the process being developed and to provide the needed process remedies more effectively.
In this work there were 8 OSP samples which failed to reach the initial 10^7 cycles requirement, all were due to micro-shrinkage porosity at the surface of the reduced gauge section. The size of these pores in non-compliant OSP samples in terms of max length range from 0.2 to 1.0 mm as shown by the red diamonds in Figure 6.

Upon review of the same figure, we can see that all compliant OSP, which ultimately did fail for micro-shrinkage porosity, had nucleating pore sizes on the fracture surface ranging from 0.3 to 1.7 mm. This was higher than for the samples which did not meet the initial 82 MPa alternating stress. This observation was also made by Mackay et al.[7] where the Staircase method and OSP method were compared. In this work, fractographic examination was performed on a total of 88 OSP samples and showed that the pore size for the samples which were compliant were similar in size range to those which were not. What was the defining factor was where the pore was located on the fracture surface. Mackay et al.[7] explained in that manuscript that upon fractographic examination, where a nucleating micro-shrinkage pore is identified, it's impossible to know the full 3-D extension of the micro-shrinkage pore, particularly above and below the fracture plane, and its overall stress concentration magnitude.

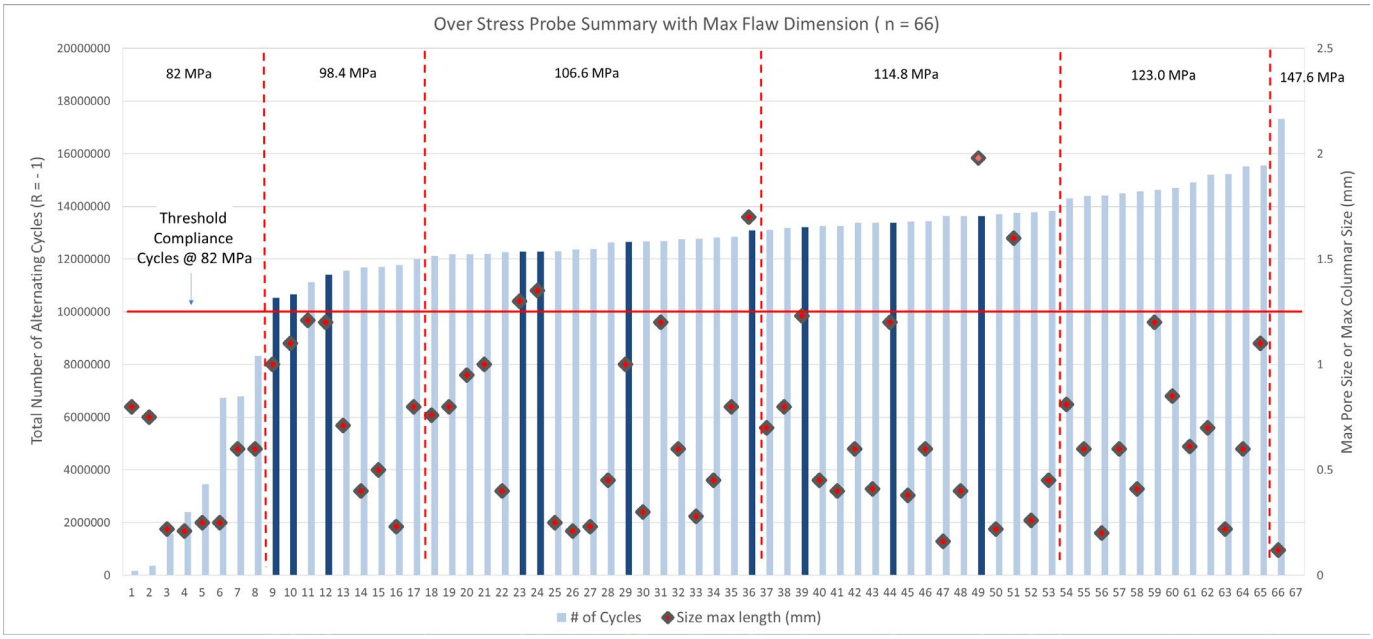

Figure 6. The summary of all 66 OSP samples tested for this study. The light blue bars represent OSP fatigue samples where fracture was nucleated by a pore, and the dark blue bars nucleation was a columnar grain. The red diamonds represent the maximum dimension of the nucleating flaw (micro-shrinkage or columnar grain).

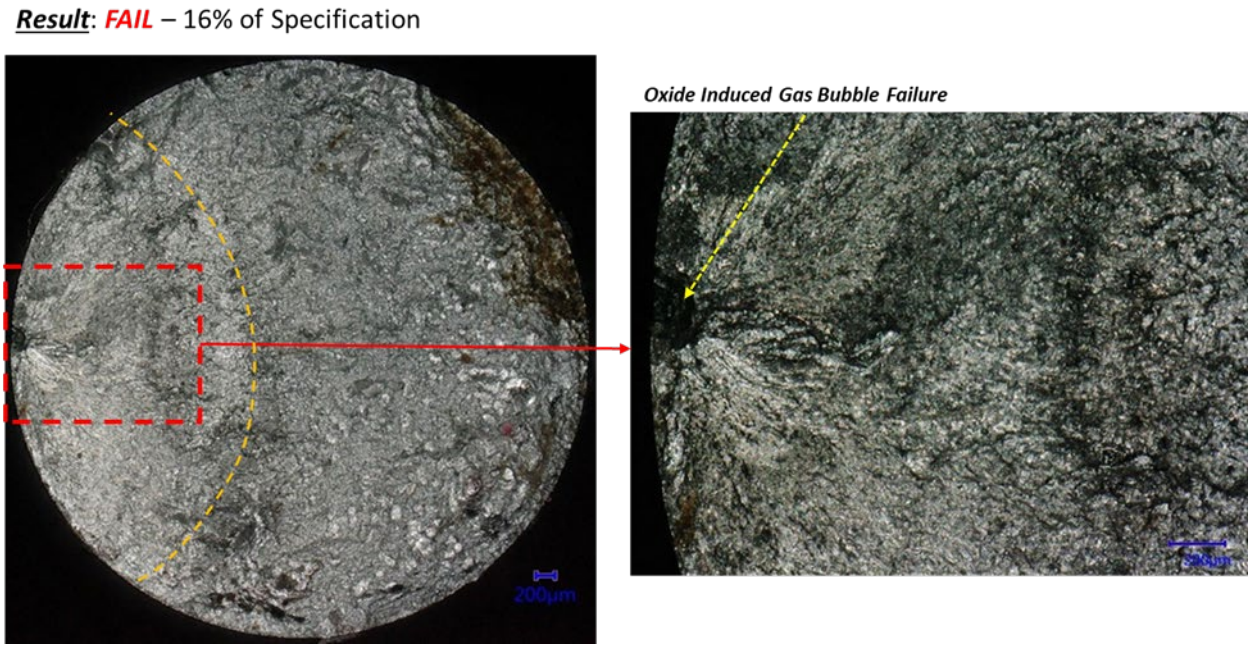

Figure 7a. The 3rd ranked OSP fatigue sample which failed at 1,561,560 cycles at 82 MPa (STP = 16%). The initiating flaw is a gas pore which has the maximum size dimension of 0.29 mm.

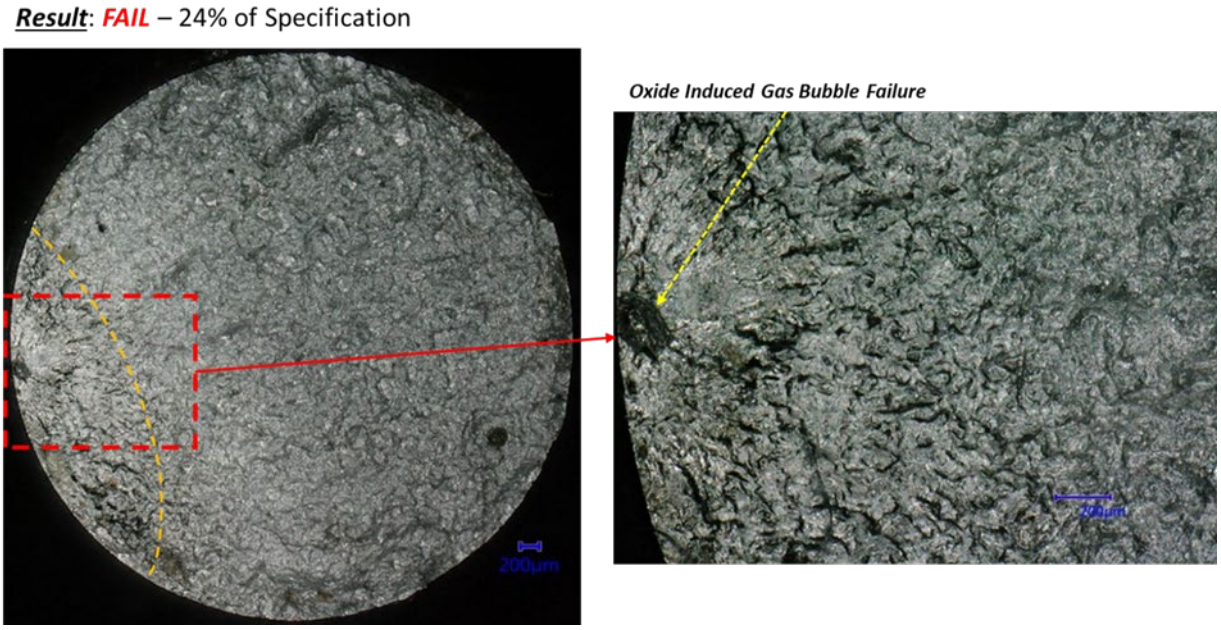

Figure 7b. The 4th ranked OPS fatigue sample which failed at 2,398,626 cycles at 82 MPa (STP = 24%). The initiating flaw is a gas pore which has the maximum size dimension of 0.27 mm.

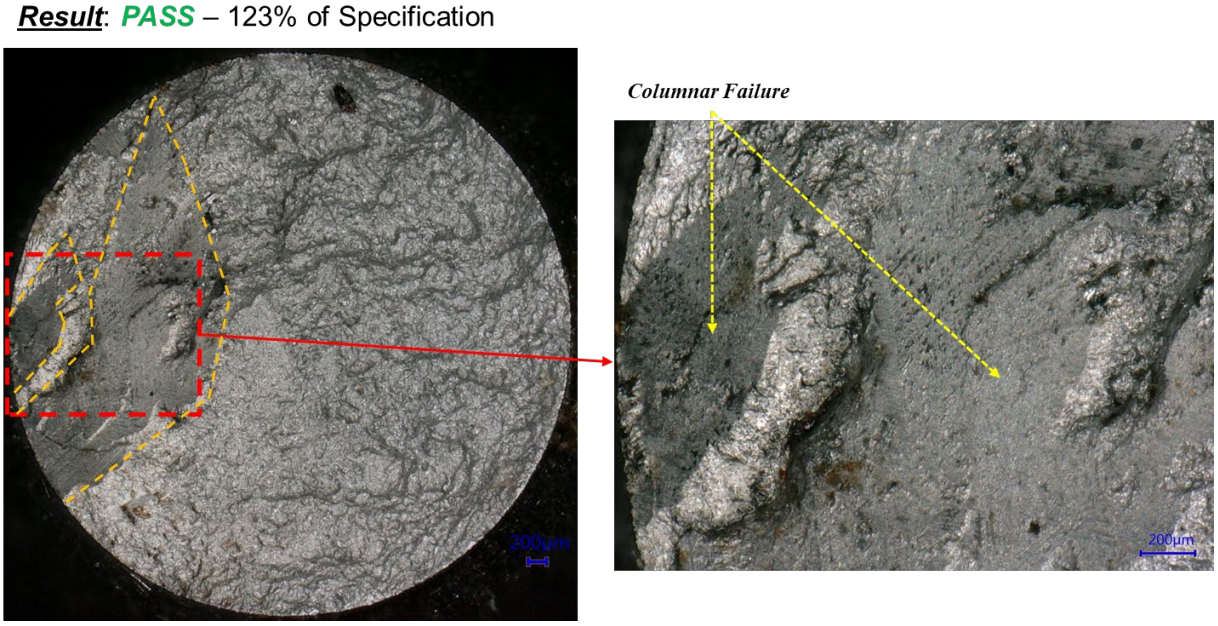

Figure 7c. The 24th ranked OSP fatigue sample which was compliant at 12,274,526 cycles at 106.6 MPa (STP = 123%). The initiating flaw is a columnar grain extends almost to the center (1.5 mm) of the sample fracture surface.

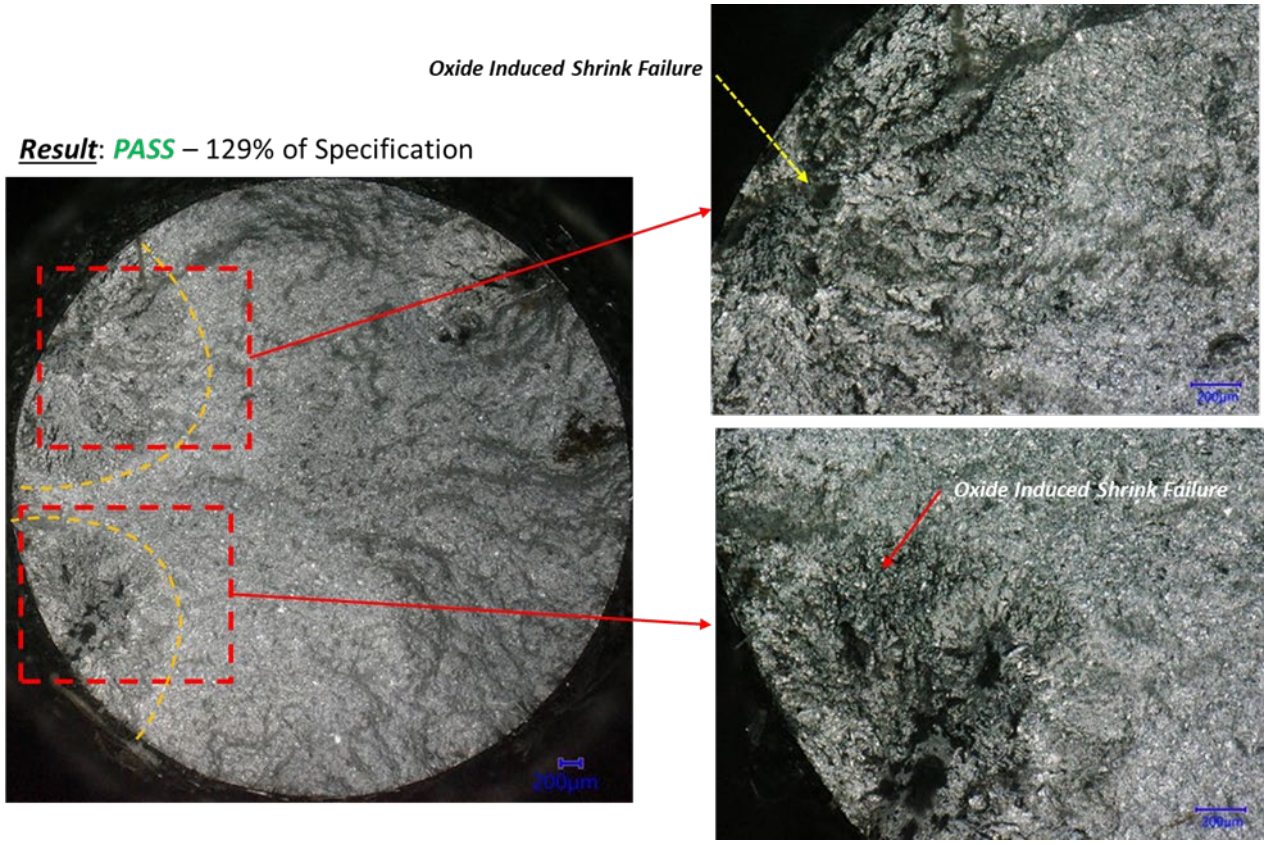

Figure 7d. The 34th ranked OSP fatigue sample which was compliant at 12,850,836 cycles at 114.8 MPa (STP = 129%). The initiating flaw is a micro-shrinkage pore which has the maximum size dimension of 0.48 mm.

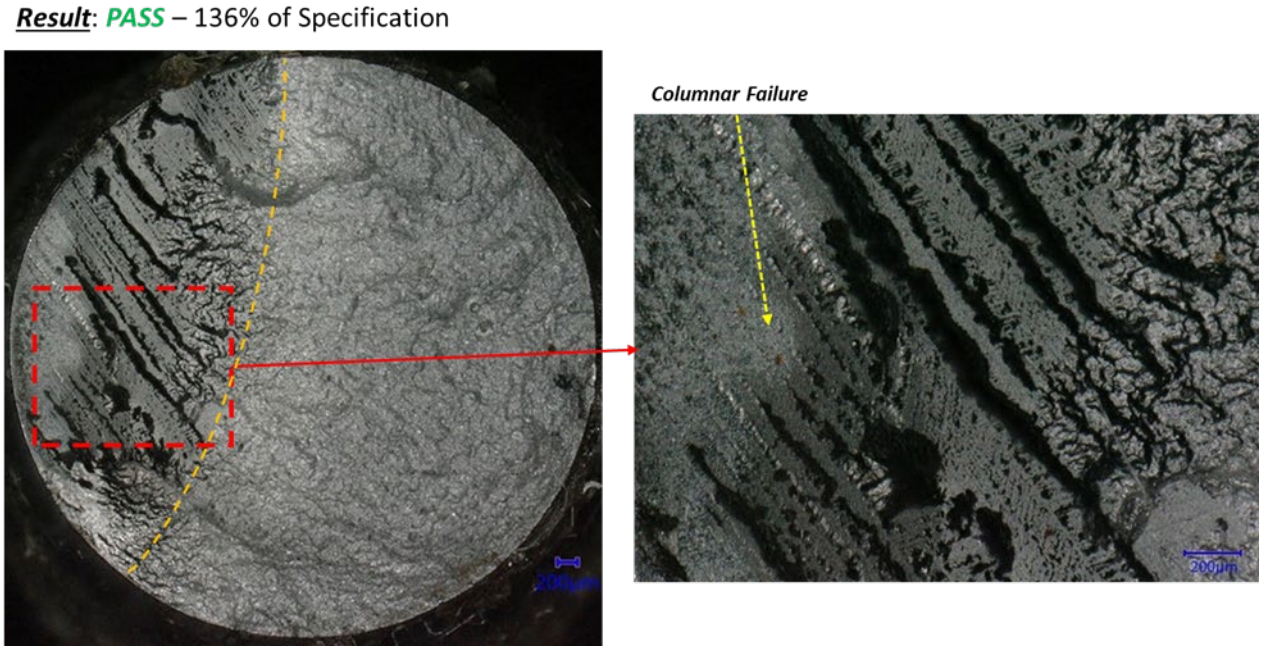

Figure 7e. The 49th ranked OSP fatigue sample which was compliant at 13,635,188 cycles at 114.8 MPa (STP = 136%). The initiating flaw is columnar grain extends almost to the center (2.5 mm) of the sample fracture surface.

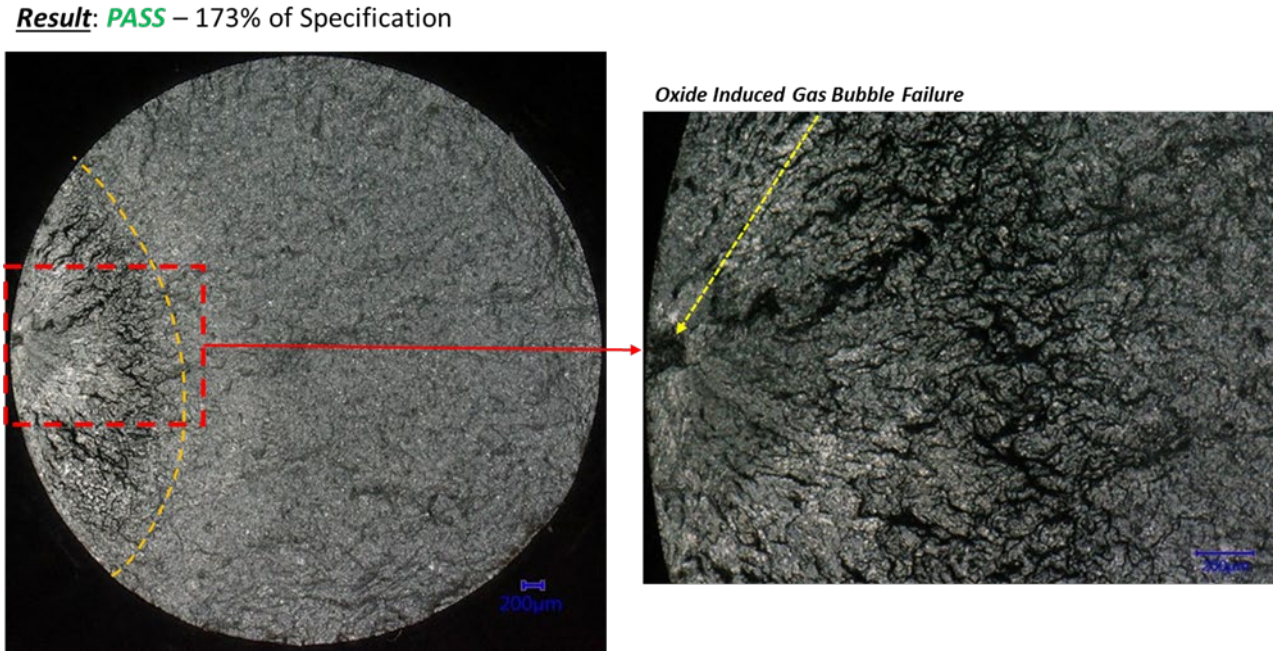

Figure 7f. The 66th ranked OSP fatigue sample which was compliant at 17,327,960 cycles at 147.6 MPa (STP = 173%). The initiating flaw is a micro-shrinkage pore which has the maximum size dimension of 0.2 mm.

In terms of the ten OSP samples which were found to have a columnar grain as the fatigue nucleation point, all exceed the 82 MPa threshold at 10^7 cycles. It's believed that this is because the fatigue bar was extracted with a portion of the columnar structure in the casting section (as alluded to in Figures 5a and 5b). The appearance of these columnar zones requires some explanation. At this point, with the absence of any other defect at the nucleation site, one must postulate that a stress concentration effect may have been present between columnar grain boundaries if oriented perpendicular to the loading condition. It is not known what portion of the slow crack advancement ($\mathbf{N_p}$ from Eqn. 1.) occupies the overall fatigue life of the sample. It would appear from the fracture surfaces of Figures 7c and 7e that the slow fracture region is completely occupied by a columnar zone feature, and then transitions straight to fast fracture ($\mathbf{N_f}$).

The non-orthogonality of the secondary dendrite arms has been reported previously by Salado-Ordorica et al.[13] which showed in their binary aluminum compositions that in very high solidification rates above 100 K/cm, secondary dendrite stems stop growing orthogonality and instead follow the heat flow at the initial stages of solidification.

Since none of the OSP samples which experienced fatigue nucleation from columnar grain boundaries failed to meet the initial threshold, should any process correction be taken? One should consider if the casting structure in which fatigue samples are taken from will have machined bolt holes or not. Fatigue failure, should it occur, will typically emerge from the trough of a thread profile, that also has a flaw, and under the tension loading portion of the cycle a crack nucleates and advances. In many cases where an aluminum casting has any cyclical tension and compression loading, roll-forming of bolt holes is usually implemented. Roll-forming has been discussed elsewhere by the authors,[7,11] but briefly it's a mechanical deformation process which forms the thread profile of the bolt hole, as opposed to drilling and tapping the bolt hole. This process, via plastic deformation, will eliminate or reduces the severity of any pore that would have been exposed at the thread profile. In terms of columnar grains, it's expected that the roll-forming process would also be implemented and be successful as the columnar grain boundary being particular to the loading direction would be destroyed. From Figure 6 we know, however, that all OSP samples which nucleated fatigue cracks from columnar grains exceeded the 82 MPa threshold which was required for compliance. However, if the alternating stress requirement changed to 95 MPa, then a small portion of the early ranked OSP samples having columnar grains as the nucleation event would have to be considered for the process corrective action. This should then drive a trial where the amount of in-mold Tibor is increased followed by checking the casting etched structure where the fatigue bar is extracted and see if the columnar zone has decreased in size and away from the fatigue bar extraction region. Should this occur then the chances of columnar fatigue failure would drop.

CONCLUSIONS

The authors have outlined an approach where all fatigue samples from a multi-fatigue test protocol are examined via fractography. Using this approach, the true pore size which has contributed to fatigue nucleation can be examined. As reported previously, those samples which did not reach the 10^7 cycles at an alternating stress of 82 MPa had a pore size, measured from metallography and from fractography, to be like those which exceeded the threshold requirement. This observation was not the first one made by the authors.[7,11] The explanation is that while the pore max sizes are measured, there is no true way to measure the sharpness of the edges of the micro-shrinkage pores seen.

Micro-shrinkage pores have complex 3-D void extensions, however using fractography, the micro-shrinkage pore can really be seen on only on a 2-D plane which is presumed to be the location of the highest stress concentration. There is no way to fully understand the extent of that micro-shrinkage pore above and below that same 2-D plane. The purpose of generating the metallographic data from below the fracture surface of fatigue samples in Figure 4 was meant to support that the basic casting structure was consistent from casting to casting. If this was not the case, where one of the metallographic results indicated a very high percentage of porosity this would have potentially indicated that the associated OSP preference would be non-compliant due to a casting filling problem.

The role of columnar grains acting as fatigue nucleation sites is a new observation made in the manuscript, however the authors are not entirely sure how rare this nucleation initiator is, as most multi-sample fatigue protocols do not have most or any of the fatigue test samples examined via fractography. A total of 10 of the 66 fatigue fracture surfaces identified as having columnar grains acting as the nucleation site but none of these samples were non-compliant.

REFERENCES

1. Francisco C. Robles-Hernandez, Jose Martin Herrera Ramirez, Robert Mackay, "Al-Si Alloys," 1st ed., Springer, Gewerbestrasse, Switzerland, pp. 237 (2017).
2. J.F. Major, "Porosity Control and Fatigue Behaviour in A356-T61 Aluminum Alloy," *AFS Transactions*, Vol. 105, pp. 901-906 (1997).

3. N.R. Green, J. Campbell, "High Reliability Aluminum Alloy Castings," *Presented at the 27th ISATA Conference*, Aachen, Germany, (Oct-Nov 1994).
4. J.E. Gruzleski & B.M. Closset, "The Treatment of Liquid Aluminum-Silicon Alloys," American Foundry Society, Inc., 256 pp. (1990).
5. J.M. Boileau, J.W. Zindel, & J.E. Allison, "The Effect of Solidification Time on The Mechanical Properties of A356-T6 Aluminum Alloys," *SAE, Paper # 970019*, SAE Warrendale, PA (1997).
6. M.J. Caton, J.W. Jones, J.M. Boileau, & J.E. Allison, "The Effect of Solidification Rate on the Growth of Small Fatigue Cracks in a Cast 319-Type Aluminium Alloy," *Metallurgical & Materials Transactions A*, Vol. 30A, pp. 3055-3068 (1999).
7. R. Mackay, G. Byczynski, "An Evaluation of the Staircase and Over-Stress Probe Methods for Fatigue Life Characterization in Aluminum Sand Castings," *International Journal of Metalcasting* (2022). https://doi.org/10.1007/s40962-021-00608-5 (Link last accessed 04-08-24.)
8. Glenn Byczynski, Robert MacKay, paper: "The Nemak Cosworth Casting Process Latest Generation," *Shape Casting: 7th International Symposium Celebrating Prof. John Campbell's 80th Birthday*, 1st Ed., TMS (The Minerals, Metals and Materials Society) pp. 179-185 (2019). DOI:10.1007/978-3-030-06034-3(Link last accessed 04-08-24.)
9. R. Mackay & G. Byczynski, "The Use of the Weibull Statistical Method to Assess the Reliability of Cast Aluminum Engine Blocks made from Different Casting Processes," Shape Casting: the Fourth International Symposium, TMS (The Minerals, Metals and Materials Society), ISBN: 978-1-11802-937-4 (2011).
10. R.I. Mackay, D. Cusinato & J.H. Sokolowski, "Chemistry Optimization to Improve Casting Durability of Engine Blocks," *International Journal of Cast Metals Research*, Vol. 23, pp. 137-149 (2010).
11. R. Mackay, G. Byczynski, J. Boileau, "An Evaluation of the Staircase and Over-Stress Probe Methods for Fatigue Life Characterization in Aluminum Sand Castings," *SAE FD&E*, (May 11, 2021).
12. M.A. Salgado-Ordorica, M. Rappaz, "Twinned Dendrite Growth in Binary Alloys," Acta Materialia (2008). https://doi.org/10.1016/j.actamat.2008.07.046 (Link last accessed 04-08-24.)